JACS
JOURNAL OF THE AMERICAN CHEMICAL SOCIETY

Article

pubs.acs.org/JACS

Ligand-Mediated "Turn On," High Quantum Yield Near-Infrared Emission in Small Gold Nanoparticles

Scott E. Crawford, Christopher M. Andolina,[‡] Ashley M. Smith,[‡] Lauren E. Marbella, Kathryn A. Johnston, Patrick J. Straney, Michael J. Hartmann, and Jill E. Millstone*

Department of Chemistry, University of Pittsburgh, Pittsburgh, Pennsylvania 15260, United States

Supporting Information

ABSTRACT: Small gold nanoparticles (~1.4−2.2 nm core diameters) exist at an exciting interface between molecular and metallic electronic structures. These particles have the potential to elucidate fundamental physical principles driving nanoscale phenomena and to be useful in a wide range of applications. Here, we study the optoelectronic properties of aqueous, phosphine-terminated gold nanoparticles (core diameter = 1.7 ± 0.4 nm) after ligand exchange with a variety of sulfur-containing molecules. No emission is observed from these particles prior to ligand exchange, however the introduction of sulfur-containing ligands initiates photoluminescence. Further, small changes in sulfur substituents produce significant changes in nanoparticle photoluminescence features including quantum yield, which ranges from 0.13 to 3.65% depending on substituent. Interestingly, smaller ligands produce the most intense, highest energy, narrowest, and longest-lived emissions. Radiative lifetime measurements for these gold nanoparticle conjugates range from 59 to 2590 μs, indicating that even minor changes to the ligand substituent fundamentally alter the electronic properties of the luminophore itself. These results isolate the critical role of surface chemistry in the photoluminescence of small metal nanoparticles and largely rule out other mechanisms such as discrete $(Au(I)—S—R)_n$ impurities, differences in ligand densities, and/or core diameters. Taken together, these experiments provide important mechanistic insight into the relationship between gold nanoparticle near-infrared emission and pendant ligand architectures, as well as demonstrate the pivotal role of metal nanoparticle surface chemistry in tuning and optimizing emergent optoelectronic features from these nanostructures.

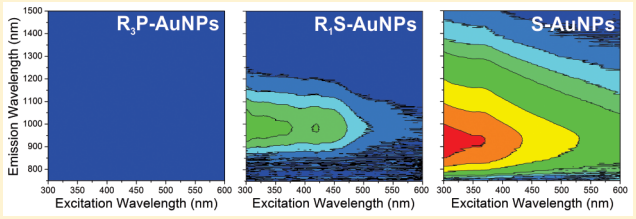

INTRODUCTION

Small metal nanoparticles (NPs) (~1.4−2.2 nm core diameters) are intriguing because they bridge molecular and bulk metal electronic structures.[1−8] One of the most interesting hallmarks of this size range is the emergence of photoluminescence (PL). The PL of gold nanomaterials is particularly interesting because emissions from the visible into the near-infrared (NIR) have been observed across a wide range of cluster and particle morphologies.[9−19] Over the past decade, it has become clear that these PL phenomena are significantly influenced by particle surface chemistry. For example, Murray and co-workers have demonstrated positive correlation between PL intensity and thiol ligand density on gold particles of various core diameters.[20] Jin and co-workers observed that PL intensity from gold clusters $(Au_{25}(SR)_{18})$ could be enhanced using thiolated ligands containing additional electron-rich atoms such as nitrogen or oxygen,[21] which are thought to change the energy of the emissive state.[22,23]

Here, we demonstrate that both thiol- and sulfide-containing binding moieties act as a "switch" that initiates PL in small gold nanoparticles (AuNPs), even in the case of unsubstituted ligands such as Na_2S. Then, the ligand substituent group can be used to fine-tune emergent PL parameters such as quantum yield (Φ) and excited state lifetimes, both by excluding nonradiative decay pathways as well as by changing the electronic structure of the luminophore itself. Interestingly, we find that the most effective ligands for optimizing PL quantum yield are also the smallest, and particles stabilized by these ligands exhibit some of the highest NIR quantum yields observed to date for metal particles at this size range. Taken together, these experiments begin to reveal the origins of PL behaviors from small AuNPs and, by extension, introduce robust methods to tailor and optimize metal NP PL properties.

EXPERIMENTAL SECTION

General Methods. 4-(diphenylphosphino)benzoic acid (4-DPPBA, 97%), hydrogen tetrachloroaurate(III) trihydrate ($HAuCl_4$, ≥ 99.9%), sodium borohydride ($NaBH_4$, ≥ 99.9%), 3-mercaptopropionic acid (MPA, ≥ 99%), 4-mercaptobutyric acid (MBuA), 6-mercaptohexanoic acid (MHA, 90%), 8-mercaptooctanoic acid (MOA, 95%), sodium sulfide nonahydrate (Na_2S, ≥ 98%), thioglycolic acid (TGA, ≥ 98%), cysteamine hydrochloride (≥ 98%), bis(p-sulfonatophenyl)phenyl phosphine dipotassium dihydrate salt (BSPP, 97%), folic acid (FA, ≥ 97%), ytterbium(III) chloride hexahydrate (99.9%), polyvinylpyrrolidone (PVP, 10 kDa), nitric acid (HNO_3, > 99.999% trace metal basis), hydrochloric acid (HCl, > 99.999% trace metal basis), 1,4-dioxane-$_{d8}$ (99 atom % D), and tropolone (≥ 98.0%) were purchased from Sigma-Aldrich (St. Louis, MO). Deuterium oxide

Received: September 5, 2015
Published: November 6, 2015

DOI: 10.1021/jacs.5b09408
J. Am. Chem. Soc. 2015, 137, 14423−14429

(99.9%) was obtained from Cambridge Isotope Laboratories (Andover, MA). 11-Mercaptoundecanoic acid (MUA) was acquired from Santa Cruz Biotechnology, Inc. (Dallas, TX). Acetonitrile (≥ 99.9% Certified ACS) and sodium hydroxide (NaOH, ≥ 97% Certified ACS) were purchased from Fisher Scientific (Waltham, MA). All reagents were used as received.

All aqueous solutions were prepared using NANOpure water (Thermo Scientific, > 18.2 MΩ·cm), and all solution were aqueous unless otherwise noted. All ligand solutions were prepared in 20.0 mM NaOH to ensure consistency across synthetic and exchange conditions. Prior to use, all glassware and Teflon-coated stir bars were rinsed with aqua regia (3:1 ratio of concentrated HCl to HNO_3) and rinsed copiously with water prior to drying in an oven. *Caution: aqua regia is extremely toxic and corrosive, and should be handled in a fume hood only, using proper personal protection equipment.*

Synthesis of 4-DPPBA-Terminated AuNPs. To a clean 250 mL round-bottom flask, 81.25 mL of water, 6.75 mL of a 10.0 mM 4-DPPBA solution, and 2.00 mL of a 20.0 mM $HAuCl_4$ solution were added, while stirring at 1150 rpm using a benchtop stir plate, under ambient conditions. After 20 s, 10.00 mL of a 20.0 mM $NaBH_4$ solution were added, producing a red-orange colloid. The solution was stirred for 1 additional min, and the particles were allowed to rest for 1 h. Afterward, the particles were centrifuged through 30 kDa molecular weight cutoff filters (Amicon Ultra-4, Millipore, Inc.) for 10 min at 4000 rcf (Eppendorf centrifuge 5804R with swing bucket rotor A-4–44). The particles were then rinsed four additional times in a 3.30 mM NaOH solution (~4 mL) to ensure that the carboxylic acid groups remained deprotonated, thereby mitigating hydrogen bond formation and/or ligand multilayer formation.[24,25] These conditions were used during all exchanges to maintain consistency between samples. Following purification, the particles were diluted with water to 1.00 mL, and 6 aliquots of 166 μL of the particles were added to separate 1.5 mL Eppendorf centrifuge tubes. To each tube, 50.0 μL of 1.00 M NaOH, 684 μL of water, and 100.0 μL of 10.0 mM thiolated ligand solution were added. The particles were then placed on a temperature controlled mixer (Eppendorf R Thermomixer), where they were mixed at 1000 rpm and 25 °C for ~16 h. After mixing, particles were again centrifuged through 30 kDa molecular weight cutoff filters for 10 min at 4000 rcf. The particles were rinsed an additional four times with 3.30 mM NaOH. All particles were characterized before and after ligand exchange by absorption spectroscopy and transmission electron microscopy (see Supporting Information for procedure details, Figures S1 and S2), as well as various NMR and PL techniques (vide infra).

Pulsed Field Gradient Stimulated Echo ^{1}H NMR. All NMR measurements were performed on a Bruker 600 Ultrashield magnet with an AVANCE III 600 or a Bruker 400 Ultrashield magnet with an AVANCE III 400 Console (Bruker Biospin, Billerica, MA). The sample temperature was controlled with a Bruker BVT3000 variable temperature system at 298 K unless otherwise stated. NMR samples were prepared by replacing the final two aqueous NaOH washes with two rinses at the same pH in D_2O during purification of the AuNPs, followed by resuspension in 10 mM NaOH prepared in D_2O. The particles were then loaded into a 5 mm NMR tube for measurement. ^{1}H NMR diffusion spectra were acquired on a broadband fluorine observe plus probe using a stimulated echo bipolar pulsed field gradient pulse sequence with WATERGATE for water suppression and dioxane as an internal standard, following our previously reported protocol.[26] Additional details, including on-particle spectra for each AuNP–ligand conjugate (Figure S3) and information regarding estimation of ligand shell thickness are provided in the SI (Figure S4, Table S1).

Method for Inductively Coupled Plasma-Mass Spectrometry Analysis. Inductively coupled plasma-mass spectrometry (ICP-MS) analysis was performed using an argon flow with a NexION spectrometer (PerkinElmer, Inc.). An aqua regia solution was prepared with a 3:1 ratio of hydrochloric acid:nitric acid and diluted with water to produce a 5% v/v aqua regia matrix. AuNP samples were taken from the concentrated pellet after ligand exchange and purification and digested overnight (~16 h) in ~5 μL of fresh and concentrated aqua regia solution. From the digested solution, 1 μL was further diluted to 5 mL using a 5% aqua regia matrix for ICP-MS analysis, while the remainder of the digest was reserved for ^{1}H NMR analysis (vide infra). Unknown Au concentrations were determined via comparison to a 5-point standard curve with a range of 1–30 ppb (1, 5, 10, 20, and 30 ppb prepared by volume) from a Au standard for ICP (Fluka, TraceCERT 999 mg ± 2 mg/L Au in HCl) diluted in the 5% aqua regia matrix. All standards were measured 5 times and averaged, while all unknown samples were measured in triplicate and averaged. A 5 min flush time with 5% aqua regia matrix was used between all runs, and a matrix blank was analyzed before each unknown sample to confirm removal of all residual metals.

Calculation of Molar Extinction Coefficient. AuNP extinction coefficients were calculated using the extinction spectrum of the AuNP suspension after purification (Cary 5000, Agilent, Inc.) but prior to digestion in aqua regia. For each ligand studied, extinction spectra were collected at five different concentrations (optical densities ranging from 0.1 to 1 at 360 nm) from 220 to 800 nm (Figure S5). The concentration of Au atoms at each particle concentration was determined by ICP-MS. For brightness calculations, extinction values were measured at 360 nm, consistent with the excitation wavelengths used. The average diameter of the NPs was determined using high resolution TEM micrographs. The total number of Au atoms was estimated per particle by dividing the volume of the AuNP sphere by the volume of the gold fcc unit cell. By dividing the ICP-MS determined Au concentration by the number of Au atoms per particle, particle concentrations were determined. Molar extinction spectra were produced from 220 to 800 nm for AuNPs capped with each ligand studied by taking the slope of the extinction versus the particle concentration for each wavelength (Figure S6).

Ligand Quantification/Ligand Density Determination by ^{1}H NMR. Ligand density measurements were conducted using our previously reported method.[24] Briefly, following ICP-MS analysis, the remainder of the digested particles was diluted to a final volume of 500 μL using D_2O, and analyzed via ^{1}H NMR. Acetonitrile (ACN, 5 μL of 0.24% v/v) was added to each sample as an internal standard. Specific proton peaks, typically those corresponding to the carbon backbone of the ligand, were integrated with respect to the ACN standard, and a five-point calibration curve ranging from 0.1 to 1 mM was prepared for each ligand considered. The signal from each sample was used in conjunction with the equation of the calibration curve to determine ligand concentrations. Particle concentrations in each sample were determined using ICP-MS and HRTEM as discussed in the calculation of molar extinction coefficient section (vide supra). Ligand densities were calculated by dividing the phosphine and thiol ligand concentrations by the concentration of particles, providing the number of thiol and phosphine ligands per particle (note that the ICP-MS and ^{1}H NMR values were always obtained from the same sample solution). Figure S7 describes the process used to determine ligand densities. Representative ^{1}H NMR spectra are included in the SI (Figures S8–S14).

Analysis of AuNP NIR Photoluminescence. The PL properties of AuNPs before and after ligand exchange were measured using a Horiba Jobin-Yvon NanoLog spectrofluorometer with a 450 W xenon source and a Symphony II InGaAs array detector. Excitation gratings were blazed at 330 nm with 1200 grooves/mm and emission gratings were blazed at 780 nm with 100 grooves/mm. All spectra were corrected for gratings, lamp, and detector response. A dark offset was used for all measurements. A 780 nm NIR cut-on filter (Oriel Instruments) was used in all measurements to block the excitation source. All samples were baseline subtracted using a scan of pure D_2O. Quartz cuvettes with 1.0 × 0.4 cm^2 dimensions (Hellma, Inc.) were used for these analyses.

Particles and standards were excited at 360 nm using an excitation slit width of 5 nm and an emission slit width of 10 nm. Emission was measured from 750 to 1500 nm, using a 30 s integration time with the InGaAs array operating in high dynamic range. Quantum yield determinations were reported relative to an ytterbium tropolone complex in DMSO (Figure S15, full method for Φ determination, see SI).[27] For emission/excitation contour maps, the excitation measurements ranged from 300 to 600 nm with 3 nm slits, and the emission

DOI: 10.1021/jacs.5b09408
J. Am. Chem. Soc. 2015, 137, 14423–14429

Table 1. Optical Properties of Ligand-Exchanged AuNPs

exchanged ligand	ε at 360 nm ($\times 10^5$ M^{-1} cm^{-1})	λ_{EM} (nm)	fwhm (nm)	Φ ($\times 10^{-3}$)	τ_{obs} (μs)	τ_{rad} (μs)	brightness ($\times 10^3$ M^{-1} cm^{-1})
4-DPPBA	10	N/A	N/A	N/A	N/A	N/A	N/A
Na_2S	6.3	877 ± 5	194 ± 5	36.5 ± 0.4	2.56 ± 0.36	59 ± 6	23
cysteamine	8.3	909 ± 3	157 ± 1	20.6 ± 0.2	2.95 ± 0.31	91 ± 16	17
TGA	9.2	875 ± 3	166 ± 8	21.8 ± 0.4	3.69 ± 0.78	82 ± 16	20
MPA	11	929 ± 5	201 ± 2	1.29 ± 0.02	1.43 ± 0.21	2590 ± 1040	1.4
MBuA	10	950 ± 3	178 ± 5	1.80 ± 0.04	1.34 ± 0.06	1240 ± 384	1.8
MHA	8.8	969 ± 3	190 ± 4	3.85 ± 0.09	1.27 ± 0.10	466 ± 160	3.3
MOA	16	936 ± 7	223 ± 8	7.81 ± 0.18	1.23 ± 0.19	150 ± 50	12.3
MUA	14	924 ± 5	235 ± 8	6.79 ± 0.13	1.56 ± 0.17	205 ± 38	9.3

All values are an average of at least 3 independent trials. N/A indicates that the values could not be measured and/or calculated. Errors are reported as standard error of the mean. Molar extinction coefficients (ε) and brightness ($\varepsilon \cdot \Phi$) were calculated from average measured values (details of these calculations and associated data are included in the SI (Figure S16)).

Table 2. Size and Ligand Shell Properties of Ligand-Exchanged AuNPs

exchanged ligand	ligands/AuNP (total #)	sulfur containing ligands[a] (%)	AuNP diameter HRTEM (nm)	AuNP hydrodynamic diameter NMR (nm)	AuNP core diameter NMR (nm)
4-DPPBA	46 ± 6	0	1.8 ± 0.3	2.9	2.1
Na_2S	N/A	45[b]	1.8 ± 0.4	2.9	2.1
cysteamine	N/A	52[b]	1.7 ± 0.3	2.2	1.7
TGA	66 ± 5	89	1.7 ± 0.3	2.9	2.1
MPA	54 ± 7	79	1.7 ± 0.3	2.8	2.0
MBuA	42 ± 1	69	1.7 ± 0.3	3.2	1.9
MHA	70 ± 11	75	1.8 ± 0.2	3.4	1.6
MOA	56 ± 5	85	1.7 ± 0.4	3.9	1.6
MUA	56 ± 9	86	1.8 ± 0.4	4.8	1.8

[a]Percent thiolated ligand is a function of the total particle ligand count. [b]For Na_2S and cysteamine, the percent thiolated ligand was determined by comparing phosphorus and sulfur XPS signals. All values are an average of at least 3 independent trials. N/A indicates that the values could not be measured and/or calculated. Errors are reported as standard error of the mean, except TEM-measured diameters, which are reported with standard deviation.

measurements ranged from 750 to 1500 nm with 3 nm slits. A 10 s integration time was used with the InGaAs array operating in high sensitivity mode.

Time-Resolved Photoluminescent Lifetimes. Measurements of the NIR time-resolved PL lifetimes were performed using a Nd:YAG Continuum Powerlite 8010 laser (355 nm, third harmonic, ~450 mJ/pulse at 10 Hz) as the excitation source. Emission was collected at a right angle to the excitation beam, and emission wavelengths were filtered using a 780 nm cut-on filter. The signal was monitored by a water-cooled Hamamatsu R316−02 photomultiplier tube coupled to a 500 MHz band-pass digital oscilloscope (Tektronix TDS 754D). Decay signals from 1000 pulses were collected and averaged. The PL decay curves were fitted with OriginPro 8.5.1 software using a biexponential decay-fitting model. A short component of 40−50 ns was observed in all collected decays, including the D_2O blanks. This short component was determined to be an artifact of the instrument and not a signal from the material in solution. The decay curves were fit using a nonlinear regression analysis, and the reduced χ^2 and R^2 values were monitored to determine the quality of the fit. At least three measurements from independent batches of AuNPs were averaged, and the standard deviation of the means are reported. For the calculation of the radiative lifetime (τ_{rad}), the Φ and the observed lifetimes (τ_{obs}) were collected from individual samples (at least three independent trials). The average τ_{rad} is reported in Table 1 with standard error.

RESULTS AND DISCUSSION

Our experiments focused on a class of aqueous AuNPs stabilized by phosphine-containing ligands. Phosphine ligand-functionalized AuNPs are ideal for these studies because they are stable,[28] do not exhibit PL, and are readily exchanged with thiolated ligands.[29] As a result, by measuring the PL of phosphine-terminated AuNPs before and after exchange with sulfur-containing ligands, we can isolate the role of the Au—S interaction in the PL mechanism, while controlling for variables such as AuNP size and shape (N.B. ligand exchange did not influence particle size or shape, Table 2 and Figures S1 and S2). The role of the ligand substituent group is similarly isolated by introducing thiol/sulfide-containing ligands differing only in parameters such as carbon chain length as well as ligands with no substituents such as Na_2S.

Following ligand exchange and purification, AuNP−ligand conjugates were characterized by a variety of techniques in order to determine AuNP size distributions (HRTEM and PFGSE-NMR), ligand densities (^{1}H NMR, ICP-MS, and HRTEM), molar extinction spectra, (ICP-MS, HRTEM, and absorption spectroscopy), and PL properties (excitation, emission, and time-resolved emission spectroscopies). The results of these studies are summarized in Table 1 and Table 2, and we discuss these data individually as a function of observed PL phenomena below.

Introduction of Sulfur-Containing Ligands "Turns On" NIR PL. Using well-described particles, PL properties of phosphine-terminated AuNPs were analyzed before and after ligand exchange. Excitation/emission spectra revealed no NIR or visible wavelength PL from 4-DPPBA functionalized AuNPs (Figure 1 and Figure S17). However, NIR PL could be initiated upon addition of sulfur-containing ligands (Figure 1). This "turn on" behavior was consistently observed using a wide variety of thiol- and sulfide-containing ligands (Table S2), including with more complex ligand systems such as proteins (Figure S18). However, ligand exchanges with nonthiolated or

DOI: 10.1021/jacs.5b09408
J. Am. Chem. Soc. 2015, 137, 14423−14429

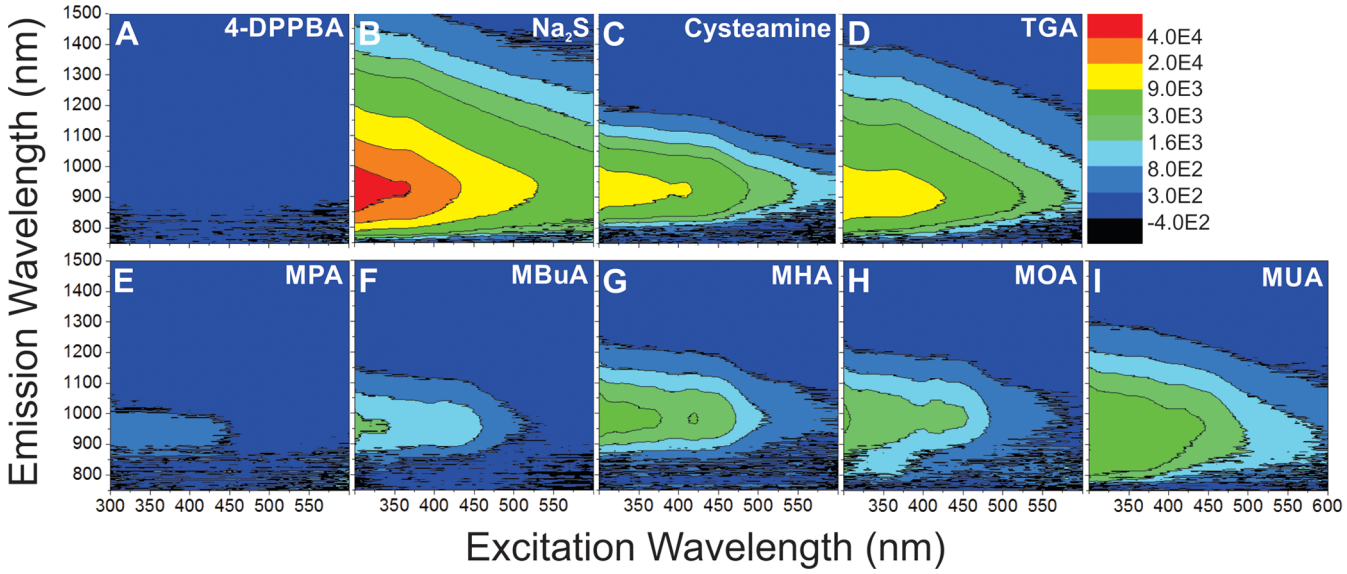

Figure 1. Excitation/emission contour maps of 4-DPPBA-terminated AuNPs before and after exchange with various thiol/sulfide-containing ligands. (A) 4-(diphenylphosphino)benzoic acid (4-DPPBA), (B) sodium sulfide (Na_2S), (C) cysteamine, (D) thioglycolic acid (TGA), (E) 3-mercaptopropionic acid (MPA), (F) 4-mercaptobutyric acid (MBuA), (G) 6-mercaptohexanoic acid (MHA), (H) 8-mercaptooctanoic acid (MOA), and (I) 11-mercaptoundecanoic acid (MUA).

thioester-containing ligands did not show any NIR PL response (Figure S19).

Significantly, this PL switching was not limited to particles initially functionalized with 4-DPPBA ligands. AuNPs synthesized with other nonthiolated ligands, including other phosphine-containing ligands such as bis(*p*-sulfonatophenyl)-phenyl phosphine (BSPP), as well as with folic acid and polyvinylpyrrolidone (PVP, 10 kDa), exhibited no PL in their as-synthesized forms. However, NIR PL responses could be introduced after ligand exchange with thiol-containing molecules (Figures S20–S22).

These data indicate that the Au—S interaction is a crucial component of NIR PL observed from AuNPs at this size range. Further, these experiments strongly suggest that the NIR PL in these systems is not the result of synthetic byproducts such as unreduced $(Au(I)—S—R)_n$ complexes.

While NIR PL is observed in all cases after thiol/sulfide-ligand introduction, large differences in quantum yield are observed depending on ligand type (up to an order of magnitude). For example, for *n*-mercaptoalkanoic acid-exchanged AuNPs, quantum yield generally increases as the length of the carbon chain increases from 3 to 11 carbons (Figure 1E–I), suggesting that larger ligands yield more emissive AuNPs (Figure 2). This relationship between ligand size and particle Φ is consistent with several studies of visible-emitting AuNPs[30,31] and is likely dependent on the ability of larger ligands to exclude collisional quenchers and other nonradiative decay pathways (e.g., excluding solvent, vide infra).

We observe notable exceptions to this trend for small ligands including thioglycolic acid (TGA), cysteamine, and Na_2S. Conjugates of AuNPs with these smaller ligands produced much higher quantum yields than their longer counterparts. For example, Na_2S-terminated AuNPs produce a Φ that is ∼540% higher than AuNPs capped with 11-mercaptoundecanoic acid (MUA). Emission from AuNPs functionalized with these smaller ligands was also higher energy (λ_{EM}, Table 1, Figure S16), more narrow (full width at half maximum (fwhm), Table 1, Figure S16), and more intense than those of AuNPs functionalized with the longer *n*-mercaptoalkanoic acids (Table 1, Figure 2). These trends are discussed in detail as a function of particle size and surface chemistry below.

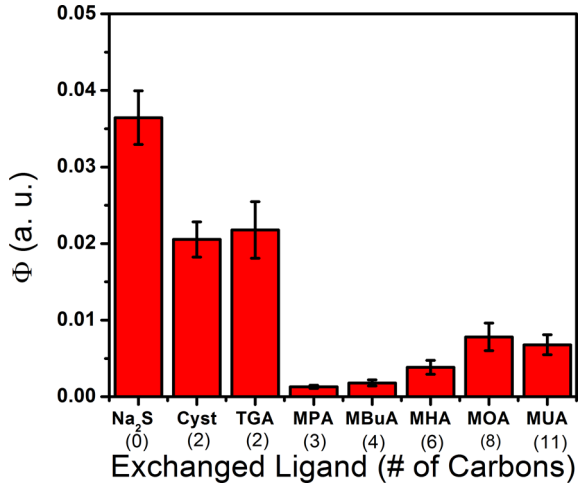

Figure 2. Quantum yield plotted as a function of ligand chain length. Error bars represent the standard error across at least five independent trials.

Ligand Density and Particle Size Do Not Explain Observed PL Differences. Because all particles are originally synthesized under identical conditions with identical ligands (4-DPPBA), they share a AuNP size distribution. However, we tested whether ligand exchange introduces particle size discrepancies as a function of ligand identity. Both HRTEM (Figures S1 and S2) and PFGSE ^1H NMR diffusion measurements confirm that there are little to no differences between core sizes before and after exchange with any of the ligands analyzed. Changes in hydrodynamic diameter can be attributed to changes in ligand length, and estimated ligand shell thicknesses are consistent with increasing ligand chain lengths from 2 to 11 carbon units with an approximately

DOI: 10.1021/jacs.5b09408
J. Am. Chem. Soc. 2015, 137, 14423–14429

constant core size (Table 2, Table S1 and Figure S4). As a result, the ligand-dependent changes in PL following ligand exchange are not attributed to changes in AuNP size.

Differences in quantum yield between different AuNP conjugates may also stem from ligand shell density. For example, it has been shown that longer *n*-mercaptoalkanoic acids tend to pack more densely than their shorter analogues on Au surfaces.[24,32] A more dense ligand shell should better protect surface excited states from collisional quenching such as solvent[33] in addition to increasing the total number of Au—S interactions, both of which are expected to produce higher quantum yields.[20] However, we observed no statistical differences in either the number of thiolated ligands or the total number of ligands between all AuNP conjugates considered (Figure 3, full statistical analysis see SI). N.B. Although MBuA-terminated AuNPs have the same total ligand density as all other samples tested, MBuA–AuNPs exhibited slightly lower thiol ligand density. Therefore, thiol ligand concentration may convolute interpretation of trends regarding MBuA-terminated NPs.

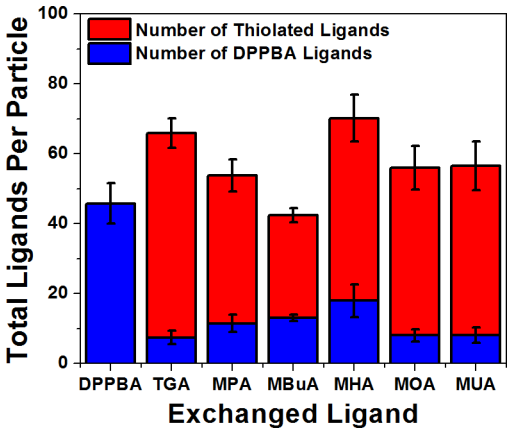

Figure 3. Total number of ligands per particle as the carbon chain length of the exchanged ligand increases (from left to right). Error bars represent the standard error of at least three measurements. (N.B. Na_2S and cysteamine could not be reliably quantified using NMR; their relative ratios were confirmed using XPS (Figures S23–25)).

Taken together, these results suggest important elements of the PL mechanism. First, despite similar thiol and total ligand densities, quantum yield varies more than an order of magnitude depending upon the length of the exchanged ligand, with the highest quantum yields observed when using the smallest ligands: TGA, cysteamine, and Na_2S. The high quantum yields observed for AuNPs terminated with these small ligands may be explained by two possible mechanisms acting either independently or simultaneously.

First, there may be fundamental differences in the Au—S binding site(s) between the smaller and larger ligands studied. For example, in solved crystal structures of Au clusters, ligands arrange in "staple" motifs where a Au atom is sandwiched between two ligand-bound sulfur atoms in various geometries.[34−36] However, in self-assembled monolayers (SAMs) on Au films, alkanethiols may adopt architectures such as the $(\sqrt{3} \times \sqrt{3})R30°$ structure observed on Au(111) surfaces.[37] Diversity in sulfur-binding environments is likely to produce distinct luminophores (whether the ligands adopt one of the two motifs cited, some combination of the two, or other motifs entirely). A second possible mechanism contributing to ligand-dependent changes in quantum yield is the orientation and arrangement of the ligands relative to the particle surface, even if the sulfur binding environment is the same. A distribution of ligand arrangements or geometries with respect to the particle surface could result in an increase in excited state deactivation pathways, dispersity in the type of luminophores and/or a decrease in the number of luminophores.

Here, we observe data that suggest an interplay between these two modes. Increases in quantum yield from particles capped by smaller ligands are consistent with the second mechanism because the quantum yield increase is accompanied by a smaller fwhm of the emission peaks. More narrow emissions suggest either more monodispersity in luminescing states and/or elimination of deactivation pathways and trap state emissions. However, we also observe seemingly two regimes of emission maxima. Small ligands (Na_2S and TGA) exhibit emission ~876 nm, whereas larger ligands (MPA through MUA) exhibit emission maxima ~942 nm (Figure S16), suggesting that there may be two distinct luminophores, consistent with the first mechanism.

Time-Resolved Photoluminescence Indicates Emissive State Involves both Au—S and Substituent Group Effects. The relationship between ligand size and quantum yield (Figure 2) cannot be explained only by steric exclusion of nonradiative decay pathways because the highest quantum yields are observed for the smallest ligands. Instead, differences in ligand identities (here, changes only in the carbon chain length) beyond the attachment moiety (i.e., thiol/sulfide) may be fundamentally changing the emissive state(s) of the particles. To distinguish these two modes, time-resolved PL decays of optically dilute samples of each AuNP–thiol/sulfide conjugate were collected in D_2O (τ_{obs}, Figure S26). From 3 to 11 carbons (MPA to MUA), τ_{obs} is approximately constant (averaged τ_{obs} = 1.37 ± 0.07 μs, Figure 4A), which is consistent with previous reports by Whetten and co-workers.[9] However, the τ_{obs} for Na_2S, cysteamine, and TGA-capped AuNPs are approximately double that of their larger analogues (τ_{obs} = 3.07 ± 0.30 μs, Figure 4A).

Using the measured values for τ_{obs} and Φ, we evaluate the radiative lifetime (τ_{rad}) of the emissive states, which describes the lifetime of the excited state in the absence of nonradiative decay pathways. Quantum yield and τ_{obs} are related by the radiative lifetime:

$$\Phi = \tau_{obs}/\tau_{rad} \quad (1)$$

If the AuNP ligands are enhancing the quantum yield solely by excluding collisional quenchers or preventing other nonradiative decay pathways, then we would expect to observe a constant value for τ_{rad} as the ligand chain length increases. However, we observe a decrease in τ_{rad} as the chain length increases from MPA to MUA (Figure 4B). This change in τ_{rad} indicates that by altering the thiol substituent, either the local chemical environment surrounding the luminophore is fundamentally changed or the luminophore itself is different in these systems.

The τ_{rad} from Na_2S, cysteamine, and TGA-terminated AuNPs again exhibit distinct behavior as compared with their longer-chain counterparts. In addition to producing narrower, more intense, and higher energy emission, these three ligands produce shorter τ_{rad} with respect to the longer ligands. These results suggest that having no functional groups adjacent to the thiol (Na_2S), or a relatively small functional group (cysteamine, TGA), induce a PL mechanism (or series of luminophores)

DOI: 10.1021/jacs.5b09408
J. Am. Chem. Soc. 2015, 137, 14423−14429

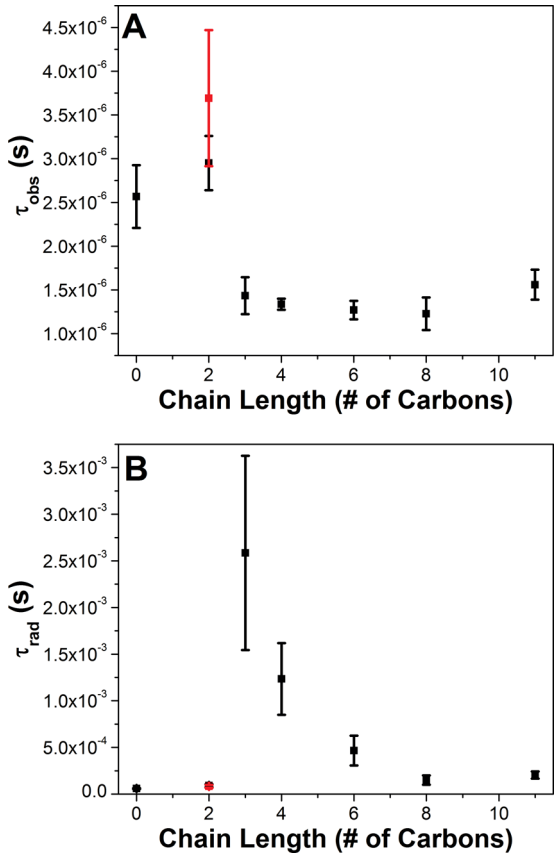

Figure 4. (A) Time-resolved observed (τ_{obs}) PL lifetimes and (B) radiative lifetimes (τ_{rad}) as a function of the number of carbons in the thiol/sulfide ligand. The red squares correspond to cysteamine-terminated AuNPs.

that is fundamentally different (or more uniform) than that produced by the longer ligands, which is consistent with changes in ligand binding motif and/or substituent interactions with the Au core, as mentioned above.

CONCLUSIONS

In summary, we report a straightforward, aqueous synthesis of small, phosphine-capped AuNPs that show no PL in the NIR. NIR PL is "turned on" by exchanging the as-synthesized ligands with thiol- or sulfide-containing ligands, which provides direct evidence that PL from AuNPs is dependent upon interactions between Au surface atoms and the ligand binding moiety. We find that the substituent group attached to the sulfur atom also plays a critical role in dictating the AuNP optical properties. For example, by increasing the ligand alkyl chain by even a single methylene unit, drastic differences in quantum yield (~1.5 orders of magnitude) are observed, despite similar core diameters and ligand densities. These observations are partially explained by ligand-dependent differences in τ_{rad}, which indicate that the ligand substituent group alters the electronic structure of the luminophore itself, likely via changes to the Au—S binding motif and/or the ligand geometry.

Importantly, Φ values observed from the small ligands (carbons $\leq$ 2) routinely exceed 2%, surpassing many of the reported values for NIR-emitting AuNPs of similar sizes[26,38−42] and even those of many lanthanide complexes.[27,43−45] The total brightness ($\varepsilon \times \Phi$) of these AuNP conjugates surpasses the highest reported brightness values for AuNPs and their alloys,[26,38] as well as many UV-sensitized lanthanide probes.[27] Taken together, these experiments elucidate important correlations between AuNP surface chemistry and their corresponding optoelectronic properties at a fundamentally important length scale between molecular and bulk metal electronic structures, in addition to introducing new strategies for the rational design of high performing NIR-emitting materials.

ASSOCIATED CONTENT

Supporting Information

The Supporting Information is available free of charge on the ACS Publications website at DOI: 10.1021/jacs.5b09408.

Contains additional synthetic details, representative HRTEM images and size distributions, all controls, description of ligand density determination, descriptions of statistical data analyses, XPS analysis, representative ^{1}H NMR spectra, representative time-resolved PL decays, and visible emission scans (PDF)

AUTHOR INFORMATION

Corresponding Author

*jem210@pitt.edu

Author Contributions

‡These authors contributed equally. All authors have given approval to the final version of the manuscript.

Funding

This work was supported by a National Science Foundation CAREER Award (CHE-1253143), the Research Corporation for Science Advancement, and the University of Pittsburgh. S.E.C. thanks the Dietrich School of Arts and Sciences at the University of Pittsburgh for the Arts and Sciences Fellowship. L.E.M. thanks the Dietrich School of Arts and Sciences for the Andrew Mellon Predoctoral Fellowship.

Notes

The authors declare no competing financial interest.

ACKNOWLEDGMENTS

We thank Prof. Alexander Star for the use of his fluorometer, Prof. Stephane Petoud for the use of his time-resolved photoluminescence decay instrumentation, and Prof. Daniel Bain for the generous use of his ICP-MS.

REFERENCES

(1) Chen, S.; Ingram, R. S.; Hostetler, M. J.; Pietron, J. J.; Murray, R. W.; Schaaff, T. G.; Khoury, J. T.; Alvarez, M. M.; Whetten, R. L. *Science* **1998**, *280*, 2098.

(2) Malola, S.; Lehtovaara, L.; Enkovaara, J.; Häkkinen, H. *ACS Nano* **2013**, *7*, 10263.

(3) Negishi, Y.; Nakazaki, T.; Malola, S.; Takano, S.; Niihori, Y.; Kurashige, W.; Yamazoe, S.; Tsukuda, T.; Häkkinen, H. *J. Am. Chem. Soc.* **2015**, *137*, 1206.

(4) Yi, C.; Tofanelli, M. A.; Ackerson, C. J.; Knappenberger, K. L. *J. Am. Chem. Soc.* **2013**, *135*, 18222.

(5) Dharmaratne, A. C.; Dass, A. *Chem. Commun.* **2014**, *50*, 1722.

(6) Koivisto, J.; Malola, S.; Kumara, C.; Dass, A.; Häkkinen, H.; Pettersson, M. *J. Phys. Chem. Lett.* **2012**, *3*, 3076.

(7) Malola, S.; Hartmann, M. J.; Häkkinen, H. *J. Phys. Chem. Lett.* **2015**, *6*, 515.

(8) Malola, S.; Lehtovaara, L.; Häkkinen, H. *J. Phys. Chem. C* **2014**, *118*, 20002.

(9) Link, S.; Beeby, A.; FitzGerald, S.; El-Sayed, M. A.; Schaaff, T. G.; Whetten, R. L. *J. Phys. Chem. B* **2002**, *106*, 3410.

DOI: 10.1021/jacs.5b09408
J. Am. Chem. Soc. 2015, 137, 14423−14429

(10) Zheng, J.; Zhou, C.; Yu, M.; Liu, J. *Nanoscale* **2012**, *4*, 4073.
(11) Zhou, C.; Sun, C.; Yu, M.; Qin, Y.; Wang, J.; Kim, M.; Zheng, J. *J. Phys. Chem. C* **2010**, *114*, 7727.
(12) Sahoo, A. K.; Banerjee, S.; Ghosh, S. S.; Chattopadhyay, A. *ACS Appl. Mater. Interfaces* **2014**, *6*, 712.
(13) Negishi, Y.; Nobusada, K.; Tsukuda, T. *J. Am. Chem. Soc.* **2005**, *127*, 5261.
(14) Jiang, J.; Conroy, C. V.; Kvetny, M. M.; Lake, G. J.; Padelford, J. W.; Ahuja, T.; Wang, G. *J. Phys. Chem. C* **2014**, *118*, 20680.
(15) Huang, T.; Murray, R. W. *J. Phys. Chem. B* **2001**, *105*, 12498.
(16) Pyo, K.; Thanthirige, V. D.; Kwak, K.; Pandurangan, P.; Ramakrishna, G.; Lee, D. *J. Am. Chem. Soc.* **2015**, *137*, 8244.
(17) Liu, J.; Yu, M.; Zhou, C.; Yang, S.; Ning, X.; Zheng, J. *J. Am. Chem. Soc.* **2013**, *135*, 4978.
(18) Guo, Y.; Wang, Z.; Shao, H.; Jiang, X. *Analyst* **2012**, *137*, 301.
(19) Wan, X.-K.; Xu, W. W.; Yuan, S.-F.; Gao, Y.; Zeng, X.-C.; Wang, Q.-M. *Angew. Chem.* **2015**, *127*, 9819.
(20) Wang, G.; Guo, R.; Kalyuzhny, G.; Choi, J.-P.; Murray, R. W. *J. Phys. Chem. B* **2006**, *110*, 20282.
(21) Wu, Z.; Jin, R. *Nano Lett.* **2010**, *10*, 2568.
(22) Parker, J. F.; Kacprzak, K. A.; Lopez-Acevedo, O.; Häkkinen, H.; Murray, R. W. *J. Phys. Chem. C* **2010**, *114*, 8276.
(23) Cirri, A.; Silakov, A.; Lear, B. J. *Angew. Chem., Int. Ed.* **2015**, *54*, 11750.
(24) Smith, A. M.; Marbella, L. E.; Johnston, K. A.; Hartmann, M. J.; Crawford, S. E.; Kozycz, L. M.; Seferos, D. S.; Millstone, J. E. *Anal. Chem.* **2015**, *87*, 2771.
(25) Kane, V.; Mulvaney, P. *Langmuir* **1998**, *14*, 3303.
(26) Andolina, C. M.; Dewar, A. C.; Smith, A. M.; Marbella, L. E.; Hartmann, M. J.; Millstone, J. E. *J. Am. Chem. Soc.* **2013**, *135*, 5266.
(27) Zhang, J.; Badger, P. D.; Geib, S. J.; Petoud, S. *Angew. Chem., Int. Ed.* **2005**, *44*, 2508.
(28) Weare, W. W.; Reed, S. M.; Warner, M. G.; Hutchison, J. E. *J. Am. Chem. Soc.* **2000**, *122*, 12890.
(29) Woehrle, G. H.; Brown, L. O.; Hutchison, J. E. *J. Am. Chem. Soc.* **2005**, *127*, 2172.
(30) Lai, S.-F.; Tan, H.-R.; Tok, E. S.; Chen, Y.-H.; Ong, E. B.; Li, M.-T.; Chen, Y.-Y.; Chien, F.-C.; Chen, P.; Margaritondo, G. *Chem. Commun.* **2015**, *51*, 7954.
(31) Chang, H.-Y.; Chang, H.-T.; Hung, Y.-L.; Hsiung, T.-M.; Lin, Y.-W.; Huang, C.-C. *RSC Adv.* **2013**, *3*, 4588.
(32) Dai, Z.; Ju, H. *Phys. Chem. Chem. Phys.* **2001**, *3*, 3769.
(33) Huang, C.-C.; Yang, Z.; Lee, K.-H.; Chang, H.-T. *Angew. Chem.* **2007**, *119*, 6948.
(34) Jadzinsky, P. D.; Calero, G.; Ackerson, C. J.; Bushnell, D. A.; Kornberg, R. D. *Science* **2007**, *318*, 430.
(35) Azubel, M.; Koivisto, J.; Malola, S.; Bushnell, D.; Hura, G. L.; Koh, A. L.; Tsunoyama, H.; Tsukuda, T.; Pettersson, M.; Häkkinen, H.; Kornberg, R. D. *Science* **2014**, *345*, 909.
(36) Hakkinen, H. *Nat. Chem.* **2012**, *4*, 443.
(37) Love, J. C.; Estroff, L. A.; Kriebel, J. K.; Nuzzo, R. G.; Whitesides, G. M. *Chem. Rev.* **2005**, *105*, 1103.
(38) Marbella, L. E.; Andolina, C. M.; Smith, A. M.; Hartmann, M. J.; Dewar, A. C.; Johnston, K. A.; Daly, O. H.; Millstone, J. E. *Adv. Funct. Mater.* **2014**, *24*, 6532.
(39) Wang, G.; Huang, T.; Murray, R. W.; Menard, L.; Nuzzo, R. G. *J. Am. Chem. Soc.* **2005**, *127*, 812.
(40) Bigioni, T. P.; Whetten, R. L.; Dag, Ö. *J. Phys. Chem. B* **2000**, *104*, 6983.
(41) Shang, L.; Azadfar, N.; Stockmar, F.; Send, W.; Trouillet, V.; Bruns, M.; Gerthsen, D.; Nienhaus, G. U. *Small* **2011**, *7*, 2614.
(42) Montalti, M.; Zaccheroni, N.; Prodi, L.; O'Reilly, N.; James, S. L. *J. Am. Chem. Soc.* **2007**, *129*, 2418.
(43) Comby, S.; Imbert, D.; Chauvin, A.-S.; Bünzli, J.-C. G. *Inorg. Chem.* **2006**, *45*, 732.
(44) Zhang, K.; Zhang, L.; Zhang, S.; Hu, Y.; Zheng, Y.; Huang, W. *Inorg. Chem.* **2015**, *54*, 5295.
(45) Shavaleev, N. M.; Accorsi, G.; Virgili, D.; Bell, Z. R.; Lazarides, T.; Calogero, G.; Armaroli, N.; Ward, M. D. *Inorg. Chem.* **2005**, *44*, 61.

DOI: 10.1021/jacs.5b09408
J. Am. Chem. Soc. 2015, 137, 14423−14429